Applied Energy 221 (2018) 112–121

Contents lists available at ScienceDirect

Applied Energy

journal homepage: www.elsevier.com/locate/apenergy

# Design of segmented high-performance thermoelectric generators with cost in consideration

Zhongliang Ouyang, Dawen Li*

*Department of Electrical and Computer Engineering, Center for Materials for Information Technology, The University of Alabama, Tuscaloosa, AL 35487, United States*

## HIGHLIGHTS

- Segmentation of high-*ZT* TE materials can offer < 1 \$ $W^{-1}$ cost-performance ratio.
- And maintaining an efficiency of 17.8% and a power density of 3 Watt $cm^{-2}$.
- The *ZT* is the top benchmark for commercial feasibility of segmented TEGs.

## ARTICLE INFO

*Keywords:*
Segmented thermoelectric generator
Compatibility
Power conversion efficiency
Output power density
Cost-performance ratio
Dollar per watt

## ABSTRACT

In this study, state-of-the-art thermoelectric (TE) materials working between 300 K and 1000 K are cautiously selected, including materials in categories of Chalcogenides, SiGe alloy, Skutterudites and Half-Heuslers. The selection principle is an overall reflection of the figure of merit (*ZT*), compatibility factors and power factors of TE materials. These chosen TE materials are divided into four groups for construction of two kinds of segmented p-type TEG legs and two kinds of segmented n-type TEG legs. Built on different combinations of these segmented TE groups, thermoelectric generators (TEGs) have been systematically modelled to find out the best cost-performance ratios and the corresponding efficiencies, output power densities and TEG geometries as well. All the TE material properties input in the simulation are temperature-dependent and the electrical & thermal contact resistances have been taken into account for every TE-TE and TE-electrode interfaces. The results demonstrate that the successful segmentation of high-*ZT* TE materials rather than their counterparts with large power factors can offer a cost-performance ratio of ~0.86 \$ $W^{-1}$, less than the commercially desired cost-effectiveness of 1 \$ $W^{-1}$, while maintaining an efficiency of 17.8% and delivering a power density over 3 Watt $cm^{-2}$. These results not only confirm *ZT* as indeed the top criterion for choosing TE materials, but also predict the commercial feasibility and competitiveness of segmented TEGs in the same dollar per watt metrics as other renewable energy sources.

## 1. Introduction

Thermal energy is widely present in every aspect of the world and the majority of it goes to waste. Thermoelectric generators (TEGs) convert heat directly into electricity through Seebeck effect [1]. As a promising renewable energy source, TEGs hold the potential to power everything from small electronics to large grids without any emission of greenhouse gas to the environment. In addition, TEGs are able to operate quietly and stably for a long time (over 30 years) without maintenance, since they are solid-state devices without moving parts [2]. The huge amount of untamed heat, if properly utilized by TEGs, can help meet the ever-increasing energy demand around the globe. However, the thermoelectric (TE) technology has only found limited number of practical applications, the most well-known ones are powering the NASA space probes [3–6]. The major issue is the low thermal-to-electricity conversion efficiency, which depends directly on the dimensionless figure of merit (*ZT*) of TE materials and the Carnot efficiency, which caps the efficiency of any heat engine, including TEGs [7]. Generally speaking, $ZT \sim 1$ is an entry-level for a TE material to be practical [8]. Larger value is preferred and gives rise to higher efficiencies. The highest *ZT* of 2.6 ± 0.3 at 923 K has been demonstrated for p-type TE materials [9]. Though most of the TE materials, especially n-type ones, possess peak *ZT* value from 1 to 2.2 in different temperature ranges [10–18]. Enhancing *ZT* value is a hard task and usually not achievable at low temperature [19]. In contrast, it is comparatively easier to augment the Carnot efficiency, which is the ratio of

* Corresponding author.
*E-mail address:* dawenl@eng.ua.edu (D. Li).

https://doi.org/10.1016/j.apenergy.2018.03.106
Received 9 December 2017; Received in revised form 5 February 2018; Accepted 26 March 2018

temperature difference between hot stage and cold stage to the temperature of the hot stage. Increasing the Carnot efficiency is usually realized by enlarging the temperature difference, indicating that more than one TE material are needed since no single TE material currently possesses high *ZT* values over a broad enough temperature range.

There are two approaches to put various TE materials into cooperation for the same TEG device. One is using multi-stage design with different electrical circuits built for various TE materials working in different temperature stages [20–22]. This method places less restrictions on the selection of TE materials but introduces heat shunts from high temperature stages directly to the load [23]. The other strategy is segmenting TE materials continuously into the same electrical circuit [24]. This tactic doesn't have thermal energy loss through shunts but imposes relatively more stringent restraints on the selection of TE materials. Snyder et al. theoretically deduced a function called compatibility factor, through which feasibility of combining two or more TE materials can be quantified [25].

With prudent choice of compatible high-performance TE materials, segmented TEGs can be quite lucrative in terms of both efficiency and output power density. In a previous work, we have shown that efficiency of over 20% and aerial power density over 2 Watt $cm^{-2}$ are possible at the temperature difference of 700 K, taking into account the effects of electrical and thermal contact resistances as well as the thermal radiation [26]. When choosing candidates for segmentation, compatibility is as important as high *ZT*. Although great effort has been made to increase *ZT*, the progress has stagnated [27,28]. A diverting part of the research passion in the field is to escalate the TE power factor, which can be simply viewed as the product of *Z* and the thermal conductivity. TE materials with larger power factor are expected to produce greater output power without necessarily higher efficiency. Compared with high-*ZT* Chalcogenides and SiGe, Skutterudites (SKDs) and Half-Heuslers (HHs) are representative TE materials of superior power factors but moderate *ZTs* [29,30]. SKDs and HHs are also promising candidates for segmented TEGs. Ngan et al. used a customized1D numerical model to estimate efficiencies of segmented TEGs with various combinations of TE materials, including HHs [31]. McEnaney et al. studied segmented model with $Bi_2Te_3$ and SKDs [32]. Zhang et al. have successfully built bismuth telluride/SKDs segmented TE modules with a current highest efficiency of 12% at a temperature difference of 541 K, matching results of their theoretical simulation [33]. In fact, most of the research projects in the TE field focus on improving the thermoelectric properties of TE materials or performance of TEG devices.

In reality, it is the cost-performance ratio rather than the high performance alone that will lead to the widespread employment of a technology. For example, photovoltaic (PV) cells have established their competence and taken large market share with their ~1 dollar per watt ($ $watt^{-1}$) cost-effectiveness. TEGs should be judged with the same metrics in order to compete with other energy sources. Yee et al. have formulated an instructive method to apply the $ per W metrics to the TEG power generation [34]. In their ensuing work, cost-performance with optimal fill factors (active cross-sectional area of TEG to area of heat exchangers) and leg lengths of 30 different TE materials has been assessed on the level of a unicouple, i.e. one pair of n-leg and p-leg, assuming same magnitude of temperature-independent Seebeck coefficients, electrical conductivity and thermal conductivity for both n- and p-type legs [35]. Due to the strong temperature-dependence of these TE material properties and the possible differences between the n- and p-type legs, the more complicated numerical approaches such as finite element method (FEM) should be implemented to more accurately evaluate the TEG performance and associated cost-effectiveness. Rezania et al. have utilized finite element analysis solver ANSYS to appraise the power per price for a unicouple system consisting of $Zn_4Sb_3$ as p-leg and $Mg_2Si_{1-x}Sn_x$ as n-leg, but their analysis does not take the cost-contribution from the heat exchanger system into account [36]. Kim et al. proposed a design with spacer inserted inside TE legs and claimed that the cost drop outpaces the reduction of the output power by performing ANSYS simulation [37]. Benday et al. analyzed the performance and economic possibility of 4 TE materials utilizing ANSYS modelling, finding out that heat sources of higher temperature are desired for improvement of financial feasibility of TEGs [38]. However, all of the above-mentioned cost-performance evaluations have not taken electrical and thermal resistances into account. More importantly, no work has been done on the cost-effectiveness of segmented TEG systems with compatible state-of-the-art TE materials to fully study their potential in practical applications.

In this study, we carefully select 10 high-performance TE materials, with 5 p-types and 5 n-types, in the category of Chalcogenides, SiGe alloy, Skutterudites and Half-Heuslers. The selecting criteria are based on an overall consideration of the TE materials for segmentation, including figure of merit (*ZT*), compatibility factors and power factors. Two p-type and two n-type segmented TEG legs are formed by the selected TE materials to generate four combinations of TEG modules. Systematical modelling of these segmented TEG modules are carried out by the 3D finite element analysis (FEA) with ANSYS. All the thermoelectric properties of the TE materials are temperature dependent, spanning a temperature range from 300 K to 1000 K, extracted directly from the published experimental data [9–18]. Contact effects at the TE-TE and TE-electrode interfaces have also been taken into account, including both the electrical and thermal contact resistances. Optimum cross-sectional area ratios ($A_n/A_p$) of TEG n-leg to p-leg have been identified for the maximal device performance, by applying the type I boundary conditions (BCs), which are the fixed temperature at hot sides (1000 K) and four different temperatures at cold sides (300 K, 323 K, 348 K, 373 K) of the TEG modules. Based on the discovered cross-sectional area ratios, optimal TEG leg lengths for the best cost-performance ratio have been found by employing type II BCs with constant temperature at hot sides (1000 K) while altering the heat transfer coefficients of cold sides. The results show that the output power density of TEGs can be enhanced conditionally by SKDs and HHs, indicating that TE materials with high power factors but relatively low *ZT*s might be preferred for applications in which cost is less important. When costs are taken into consideration, including materials, heat transfer and manufacturing cost, TE materials of higher *ZT*s demonstrate notable advantages over their counterparts with higher power factors. The successful segmentation of high-*ZT* TE materials is able to offer a cost-performance ratio of ~0.86 $ $W^{-1}$, while maintaining an efficiency of 17.8% and delivering a power density of over 3.0 Watt $cm^{-2}$. On the other hand, segmented TE modules involving TE materials with larger power factors can only provide a cost-performance ratio of ~1.11 $ $W^{-1}$, corresponding efficiency of 16.2% and power density of ~2.4 Watt $cm^{-2}$. These results confirm that *ZT* is indeed the top benchmark for selecting TE materials. More importantly, the low dollar-per-watt values along with the high efficiencies and power densities make it possible for segmented TEGs to be competitive with other renewable energy sources such as photovoltaic cells.

## 2. Method

### 2.1. Governing equations of TEG physics

When the system arrives at a steady state, the heat flux $\vec{q}$ ($W \cdot cm^{-2}$) absorbed at the hot side of the TEG module and the current density $\vec{J}$ ($A \cdot cm^{-2}$) flows in the TEG legs can be expressed as follows [1],

$$\vec{q} = T\alpha\vec{J} + \kappa\vec{\nabla}T \tag{1}$$

$$\vec{J} = \frac{1}{\rho}(\vec{E} + \alpha\vec{\nabla}T) \tag{2}$$

where $\alpha$, $\rho$, $\kappa$, $\vec{E}$ and $T$ are the Seebeck coefficient, electrical resistivity, thermal conductivity, electrical field and absolute temperature,

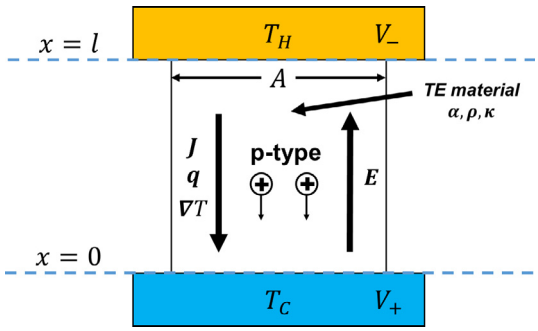


**Fig. 1.** Schematic of the thermoelectric operation and parameter denotation.

respectively. The sign convention of each vectors are shown in Fig. 1. Here a 1D denotation is used for the analytical deduction in a single p-type TEG leg, while the 3D form is used for couples of p-type and n-type TEG legs in the numerical simulation by ANSYS.

Eq. (1) shows that the total heat (power) absorbed equals Peltier heat (power) generated, plus Fourier heat (power) transferred. Eq. (2) expresses a modified Ohm's law by taking Seebeck effect into account. Assuming $T_H - T_C = \Delta T \to 0$, Eq. (1) can be approximated by Eq. (3) and the overall efficiency of TEG can be denoted by Eq. (4).

$$q = \left(T_H \frac{\alpha^2}{\rho} + \kappa\right)\frac{\Delta T}{l} \tag{3}$$

$$\eta_{max} = \frac{T_H - T_C}{T_H}\left(\frac{\sqrt{1+Z\overline{T}} - 1}{\sqrt{1+Z\overline{T}} + \frac{T_C}{T_H}}\right) \tag{4}$$

In Eq. (3), $l$ is the length of TEG leg and $\alpha^2\rho^{-1}$ is the so-called TE power factor (P.F.) of the TE material. In Eq. (4), $Z = \frac{\alpha^2}{\rho\kappa}$ and $Z\overline{T}$ is the average figure of merit in the range between the hot-side temperature $T_H$ and the cold-side temperature $T_C$. Eq. (3) shows clearly that the heat flux at hot side is influenced by the power factor, thermal conductivity, temperature difference and the length of the TEG leg, without explicit dependence on the cross-sectional area. In order to maximize the efficiency in Eq. (4), two additional requirements need to be met, as indicated in formulas below [19].

$$\beta = \frac{R_L}{R} = \sqrt{1+Z\overline{T}} \tag{5}$$

$$\frac{A_n}{A_p} = \sqrt{\frac{\rho_n \kappa_p}{\rho_p \kappa_n}} \tag{6}$$

Eq. (5) is the relation between external load resistance $R_L$ and the TEG inner resistance $R$ that yields the highest efficiency, as compared with the relation $R_L = R$, which produces the maximum output power. From our previous work, we found that the following modification of Eq. (6) is convenient for estimating and choosing the initial cross-sectional area of the TEG legs before conducting actual simulation on segmented TEGs [26].

$$\frac{A_n}{A_p} = \overline{\sqrt{\frac{\rho_n(T)\cdot\kappa_p(T)}{\rho_p(T)\cdot\kappa_n(T)}}} = \left(\sum_{T_C}^{T_H}\sqrt{\frac{\rho_n(T)\cdot\kappa_p(T)}{\rho_p(T)\cdot\kappa_n(T)}}\Delta T\right)\Big/(T_H - T_C) \tag{7}$$

### 2.2. Cost–performance metrics

The cost-performance $C.\ P.$ of a TEG can be defined as the ratio of the overnight capital cost $C_{tot}$ to the power generation capability $P$ of the TEG, expressed by Eq. (8) with the unit of dollar per watt ($\$\,W^{-1}$).

$$C.\ P. = \frac{C_{tot}}{P} = \frac{\Omega_g D l A_{TE} + \Omega_{M,g} D l A_{TE} + \Omega_{M,A} A_{TE} + \Omega_{HX} h A_{HX}}{\eta A_{TE} q} \tag{8}$$

The overnight capital cost comprises (i) the cost of TE materials, (ii) manufacturing costs of the TE module and (iii) the cost of heat exchangers on both sides. The cost of a TE material is the product of this material's gravimetric price $\Omega_g$ ($\$\,kg^{-1}$), its density $D$, length $l$ and cross-sectional area $A_{TE}$. Manufacturing costs are composed of the gravimetric manufacturing cost with a price of $\Omega_{M,g}$ ($\$\,kg^{-1}$) and areal manufacturing cost with a price of $\Omega_{M,A}$ ($\$\,cm^{-2}$). The former refers to the processing such as hot pressing, ball milling, etc., scaling with the weight of TE materials. The areal manufacturing cost involves processing like soldering, metallization, cutting and dicing, scaling with the active cross-sectional area of the TEG module. The cost of heat exchangers is the product of the unit price $\Omega_{HX}$ ($\$\,W^{-1}\,K$), heat transfer coefficients $h$ ($W\,m^{-2}\,K^{-1}$) and the cross-sectional area $A_{HX}$ of heat exchangers. The power generation capability $P$ of the TEG is more straightforward, being the product of the TEG efficiency $\eta$, cross-sectional area $A_{TE}$ and the heat flux $q$ absorbed at the hot side. By utilizing expressions in Eq. (3) and defining the fill factor $F = A_{TE}/A_{HX}$, Eq. (8) can be simplified to Eq. (9), which is a quadratic equation of variable $l$ since no other parameter has explicit dependence on the TEG leg length. This indicates that the TEG cost-performance ratio has a minimum at an optimal $l$ value. Although Eq. (9) is for a TEG with a single leg, such a behavior is expected to be universal to any TEG module, including TEGs with multiple segmented p & n legs. In case of segmented TEGs, the cost for each individual TE materials is calculated first, then their contributions are summarized to the total cost.

$$C.\ P. = \frac{(\Omega_g + \Omega_{M,g})DFl^2 + (\Omega_{M,A}F + \Omega_{HX}h)l}{\eta F(T_H\frac{\alpha^2}{\rho} + \kappa)\Delta T} \tag{9}$$

$$(\Omega_g + \Omega_{M,g})_i D l A_{TE} = A_p \sum_i (\Omega_g + \Omega_{M,g})_i D_{p,i} l_{p,i} + A_n \sum_j (\Omega_g + \Omega_{M,g})_j D_{n,j} l_{n,j} \tag{10}$$

As exhibited in Eq. (10), for example, the cost of $i$ th p-type TE material equals the product of its collective price $(\Omega_g + \Omega_{M,g})_i$, density $D_{p,i}$ length $l_{p,i}$ and cross-sectional area $A_p$ in the p-leg. It should be noted that the minimal cost-performance is calculated from Eqs. (8) and (10) rather than Eq. (9), which is only deduced for theoretical analyzing purpose. The optimal leg length, output power and heat transfer coefficients are all obtained by simulation, while $A_{TE}$, $A_n$, $A_p$ and $A_{HX}$ will be discussed more in a later section. The densities and gravimetric prices of various TE materials [9–18] are extracted from literatures and listed in Table 1 [35,39]. Some TE materials do not have exact prices published, therefore assuming the prices of the most similar ones will still yield a fairly accurate result. Meanwhile, the prices of manufacturing and heat exchangers are listed in Table 2 [34,35,40]. Although being fabricated via different methods, all of 10 selected TE materials are bulk processed, and thus estimated to have the same fabricating price for simplicity, i.e., 2.4 $\$\,kg^{-1}$ (ball milling + spark plasma sintering) for gravimetric manufacturing price and

**Table 1**
Densities and prices of TE materials used in this study [9–18,35,39].

| Material name | Density $D$ ($g\,cm^{-3}$) | Gravimetric material prices $\Omega_g$ ($\$\,kg^{-1}$) |
|---|---|---|
| $(Bi,Sb)_2Te_3$ | 6.4367 | 125.47 |
| MgAgSb | 6.2 | 114 |
| $PbTe_{0.7}S_{0.3}$ | 7.07 | 83.81 |
| SnSe | 6.1 | 83.81 |
| H-doped SnSe | 6.1 | 83.81 |
| $CuxBi_2Te_{2.7}Se_{0.3}$ | 7.77 | 171 |
| $AgPb_mSbTe_{2+m}$ | 9.27 | 83.81 |
| $Si_{80}Ge_{20}$ | 2.8 | 371 |
| $Yb_{0.3}Co_4Sb_{12.2}$ | 7.48 | 64 |
| $Ti_{1-x}Hf_xNiSn_{1-y}Sb_y$ | 9 | 166 |

**Table 2**
TEG manufacturing cost and heat exchanger prices used in this study [34,35,40].

| | |
|---|---|
| Gravimetric manufacturing price $\Omega_{M,g}$ ($\$\,kg^{-1}$) | 2.4 |
| Areal manufacturing price $\Omega_{M,A}$ ($\$\,cm^{-2}$) | $1.68 \times 10^{-2}$ |
| Heat exchanger price $\Omega_{HX}$ ($\$\,W^{-1}\,K$) | 2.05[a] or 10 |

[a] Possible price at large-scale production and installation.

$1.68 \times 10^{-2}\,\$\,cm^{-2}$ for areal module price [35]. The segmentation of TE materials is usually achieved by soldering [41,42], which will increase the total areal manufacturing cost. For example, one TEG leg with N segments of different TE materials will require N − 1 times of soldering jobs in addition to the regular soldering/metallization of the electrodes. As a result, the areal cost for this segmented TEG leg approximately equals to the product of the number N, the cross-section area of the leg and the areal manufacturing price. At present, the unit price of the heat exchangers is $\sim 10\,\$\,W^{-1}\,K$ and dominates the total cost of the TEG system. However, current high prices can be significantly reduced by the large scale production and installation, providing a value of $\sim 2.05\,\$\,W^{-1}\,K$ for the unit price of heat exchangers $\Omega_{HX}$, which contains prices of both heat exchangers and ceramic plates [34]. It is worth noting that any operating cost is excluded since the cost-performance ratio in this context is calculated as the overnight capital cost versus the TEG output power. Operating cost such as the circulation of cooling water is more appropriate for calculation of the $ per kWh metrics and therefore is not in the scope of this study.

### 2.3. Properties of segmented TE materials and contact resistances

Our choice of TEG leg materials contains two general p-type groups and two general n-type groups. P-type 1 is the combination of current best p-type materials in terms of *ZT*, including $(Bi,Sb)_2Te_3$, MgAgSb, $PbTe_{0.7}S_{0.3}$ and the un-doped SnSe for operating temperatures of 300–400 K, 450–500 K, 550–800 K and 850–1000 K, respectively [9–12]. P-type 2 is constructed by replacing $(Bi,Sb)_2Te_3$, MgAgSb and $PbTe_{0.7}S_{0.3}$ in P-type 1 with the hole-doped SnSe [13]. For n-type 1 group, $CuxBi_2Te_{2.7}Se_{0.3}$ are selected for low temperature, $AgPb_mSbTe_{2+m}$ for medium temperature and $Si_{80}Ge_{20}$ for high temperature ranges, representing the current best n-type combination in terms of *ZT* [14–16]. The Yb-filled SKD ($Yb_{0.3}Co_4Sb_{12.2}$) is teamed up with the $Ti_{1-x}Hf_xNiSn_{1-y}Sb_y$ HHs to make up n-type 2 group, denoting the present top n-type combination in terms of power factors [17,18]. In total, four types of TEGs are constructed, including assemblies of "p-type 1 + n-type 1", "p-type 1 + n-type 2", "p-type 2 + n-type 1" and "p-type 2 + n-type 2". The compatibility factors of the TE materials are calculated before selection to guarantee these TE materials would collaborate with each other in each group combination and leg construction, enhancing instead of adversely affecting the overall TEG performance. Fig. 2 shows a detailed *ZT* values of the chosen 10 TE materials at different working temperature ranges, including two p-type groups (a) and two n-type groups (b). Fig. 3a and b illustrate temperature dependence of the compatibility factors for all the chosen TE materials. The solid symbols represent type 1 TE materials, either p-type or n-type, while hollow symbols represent TE materials for type 2 collections of TE materials. It can be seen that the compatibility factors are in smooth transitions in the range of 300–1000 K for both the two p-type and the two n-type segmented legs. For example, the components of n-type 2, including Yb-SKD and the Half-Heuslers, have compatibility factors changing smoothly between $-4\,V^{-1}$ and $-2\,V^{-1}$ without any abrupt break. Fig. 3c and d shows power factors of the selected TE materials versus temperature. The power factors of the p-type 2 is similar to that of the p-type 1, while the power factors of the n-type 2 is apparently much larger as compared to the n-type 1. It is worth pointing out that neither the figure of merits *ZT* nor the compatibility and power factors are entered in the simulation. However, TE properties like Seebeck coefficients, electrical resistivities and thermal conductivities are put directly into the simulation, all of which are also temperature dependent and extracted from respective literatures [9–18]. Copper is adopted for electrodes, whose thermal and electric properties varies with temperature as well and can be found in a previous work [26]. The ceramic substrates that sandwich the TE modules assume standard alumina ($Al_2O_3$) with thermal conductivity of $30\,W\,m^{-1}\,K^{-1}$ [36].

The electrical and thermal contact resistances are inevitable in any TEG module. If not well-controlled, these contact effects can be detrimental to the performance of TEGs [26]. Compared with thermal contact resistance, electrical contact resistance inflicts more serious impact on both the efficiency and output power density of TEGs. Several recent sources have reported that electrical contact resistances on the order of magnitude of $10^{-10}\,\Omega\cdot m^2$ are obtainable, which reveals the practicability of creating high-quality interfaces [33,43–45]. In this study, more conservative electrical contact resistance of $1 \times 10^{-9}\,\Omega\cdot m^2$ is applied along with thermal contact resistance of $1 \times 10^{-6}\,m^2\cdot K\cdot W^{-1}$ for both the segment-segment and segment-electrode interfaces. The thermal contact resistance between the TEG and cooling system is assumed to be ideal. In fact, Zhang et al. has demonstrated that the thermal contact resistance between TEG and cooling system is not a problem if well-managed [33]. In addition, thermal radiation and convection are also not considered in the modelling because such loss can be largely prohibited by filling and encapsulation.

### 2.4. TEG module geometries

All of the TEG modules in this study are constructed with two unicouples which are connected electrically in series but thermally in

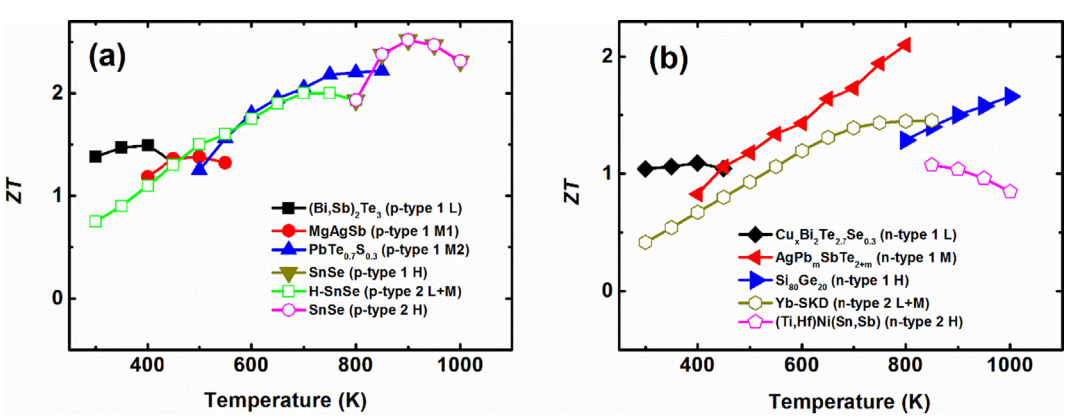


**Fig. 2.** *ZT* values of (a) p-type and (b) n-type segmented TE materials at different operating temperature ranges. L, M, H denote low, medium and high temperatures, respectively [9–18].

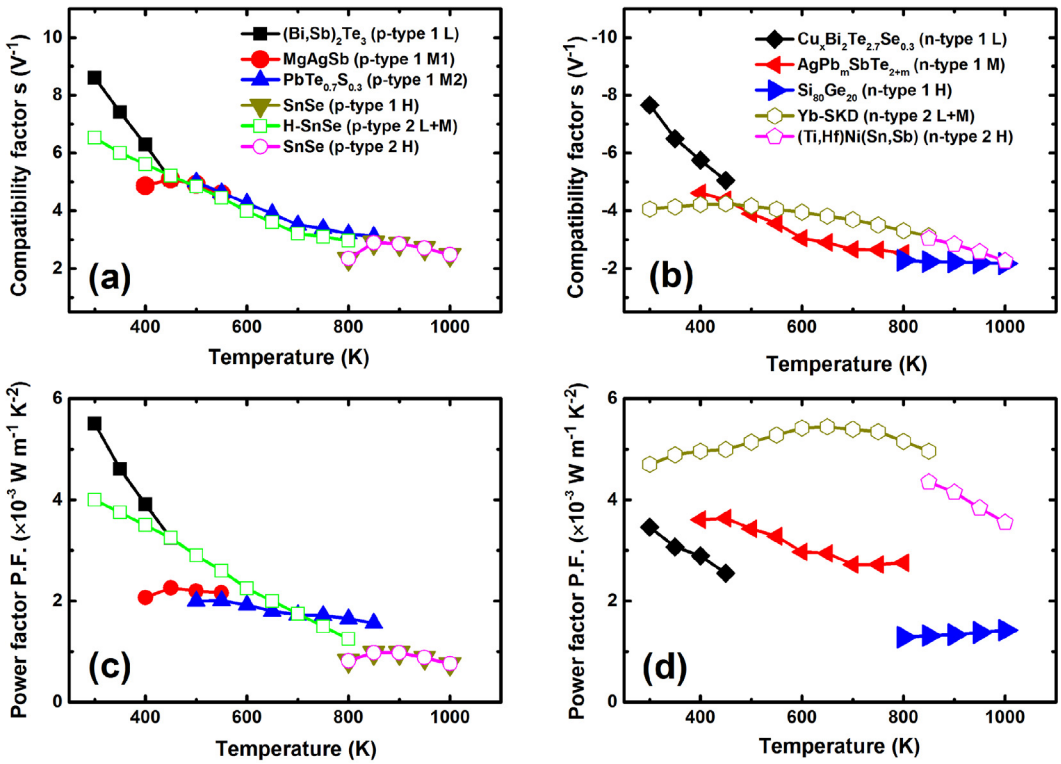


**Fig. 3.** Compatibility factors (a) & (b) and power factors (c) & (d) for p-type group 1 & group 2 and n-type group 1 & group 2, respectively [9–18].

parallel. Non-symmetrical leg geometries are employed to maximize the performance of TEG modules, due to the fact that n-type TE materials are universally weaker compared with their p-type counterparts. To be specific, the cross-sectional area of n-legs is smaller than the p-legs for realizing both the highest efficiency and the largest output power density. First, optimal ratios of $A_n$ to $A_p$ has been investigated, where $A_n$ and $A_p$ are cross-sectional areas of a single n-leg and p-leg, respectively. At this stage, the length of TEG legs is kept constant at 1 cm. The $A_p$ is fixed at 1 cm × 1 cm throughout all the simulation, including the optimization of the leg length that will be discussed later. 1 cm × 1 cm cross-sectional area may seem large for one leg. The actual manufacturing usually utilizes a large number of TEG legs with small cross-sectional area to generate high output voltage for practical applications. It has been shown that with the same total active cross-sectional area and leg length of TEGs, the number of the legs should have negligible effect on both the efficiency and the output power density [26]. The TEGs used in this study with four legs each of 1 cm × 1 cm dimension could have overall equal cross-sectional areas, resulting in the same amount of TE materials used. Based on Eq. (7), a trial optimal $A_n/A_p$ ratio for the highest efficiency is predicted for every assembly of p-type & n-type legs. This serves as a starting point, around which more points are assigned for simulation which attempts to find extremes for both the efficiency and output power density. Taking "p-type 1 + n-type 1" for example, the trial value of $A_n/A_p$ ratio is calculated as 0.682, corresponding to an n-leg dimension of ~0.82 cm × 0.82 cm. An amending step of 0.02 cm is executed on the width of the n-leg, giving dimensions from 0.7 cm × 0.7 cm to 1.12 cm × 1.12 cm. Although the n-leg with dimensions over 1 cm × 1 cm are not necessary for tracing the maximal efficiency and power density, they are included here to offer better visual effect on the trend. During the process, the thicknesses of segmentations have been simulated iteratively to make sure that each material works in its designated temperature range. After identifying the largest output power density, the corresponding $A_n/A_p$ ratio is kept unchanged for further optimization of the TEG leg length. The thickness of copper electrodes is 0.03 cm, which is not used in valuation of copper cost since the areal manufacturing cost has already been accounted for. Similar situation applies to the ceramic plates' thickness of 0.05 cm, owing to the inclusion of ceramic plates' expenses into the price of heat exchangers $\Omega_{HX}$. The horizontal dimension of ceramic plates is chosen to be 3 cm × 3 cm, giving a cross-sectional area $A_{HX}$ of 9 cm$^2$.

## 3. Results and discussion

### 3.1. Optimization of the $A_n/A_p$ geometrical ratio

At this stage, type I boundary conditions (BCs) are applied with hot sides and cold sides of TEG modules set to 1000 K and 300 K, respectively. With TEG leg length $l$ = 1 cm and $A_p$ = 1 cm × 1 cm, varying the $A_n/A_p$ ratio is actually altering the cross-sectional area of n-type legs. For each set of $A_n$ and $A_p$, both the efficiency and output power density can be maximized with respective external load conditions, i.e., $R_L/R = \sqrt{1 + Z\overline{T}}$ for the efficiency and $R_L = R$ for the output power density. The effect of an external load is simulated by changing the potential difference between two electrodes. In order to get the optimal $A_n/A_p$ ratio, dynamic adjustment is needed simultaneously for two classes of parameters, including the magnitude of the external load and the thickness of each TE segment. Fig. 4 shows the typical current-voltage (I-V) curve and current-dependency of the TEG efficiency and output power density. Through modifying the potential difference V and iterative adjustment of the thickness of every segmentation, the highest efficiency and maximum output power density can be obtained for each $A_n/A_p$ ratio by making sure that each TE material works in its designated temperature range. Fig. 5a illustrates one of the constructed TEG modules utilized in this work with two p-type segments and three n-type segments, corresponding to the assembly of "p-type 2 + n-type 1". Fig. 5b demonstrates the modelled temperature distribution in the same TEG module.

Since the maximum output power is directly related to the estimation of cost-performance ratio, i.e. dollar per watt, the maximum output power density at each $A_n/A_p$ geometrical ratio and corresponding efficiency are displayed in Fig. 6. All four assemblies of "p-type 1 + n-type 1" (Fig. 6a), "p-type 2 + n-type 1" (Fig. 6c), "p-type 1 + n-type 2"

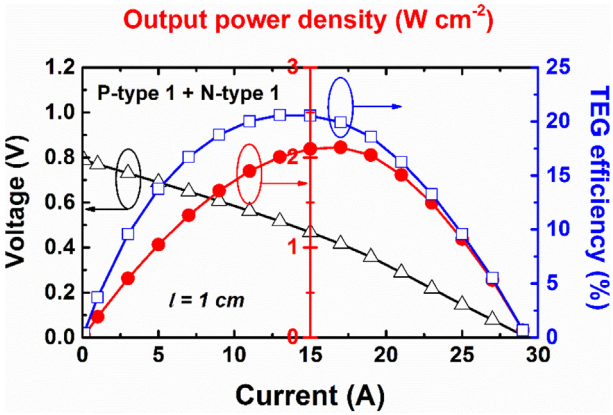


**Fig. 4.** Typical current-dependency of the output voltage, efficiency and output power density in a segmented TEG.

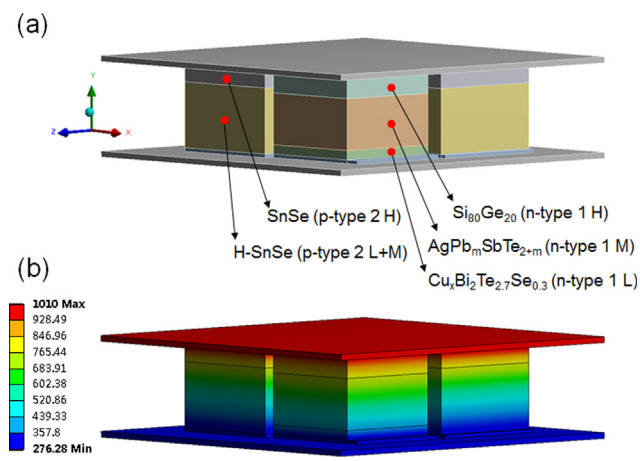


**Fig. 5.** (a) Modelling example of segmented TEG modules, and (b) the corresponding temperature distribution.

(Fig. 6b) and "p-type 2 + n-type 2" (Fig. 6d) could provide peak output power densities of 2.14, 2.24, 2.55 and 2.72 Watt cm$^{-2}$, respectively. With different assemblies, the largest output power densities occur at different $A_n/A_p$ ratios, verifying that the adoption of uniform cross-sectional areas for TEG legs ($A_n = A_p$) is not beneficial to the TEG performance. Also from Fig. 6, it can be observed that the largest output power densities come from TE materials with greater power factors but relatively lower *ZT*s (n-type 2) and the higher efficiency does not guarantee the larger output power density, given that the boundary conditions are fixed temperature at both the hot side and cold side of TEGs. For example, TEGs with n-type 2 (Yb-filled SKD + HHs) could produce ~20% more power over TEGs with n-type 1 (Chalcogenides and SiGe), even although the efficiencies are 2 percentage points lower. This can be better understood by comparing the results in Fig. 6 with the *ZT*s and power factors of different TE materials shown in Figs. 2 and 3, respectively. While the *ZT*s of Yb-filled SKD and HHs are universally weaker, their power factors are considerably larger throughout the entire temperature range in the study, giving them an edge on power generation. According to Eq. (3), with their superior power factors, Yb-filled SKD and HHs will induce greater heat flux absorbed at hot sides of TEGs. At the same time, thermal energy expelled at the TEG cold sides is also expected to be significantly faster, implying the requirement of better heat exchangers. In reality, the cost of heat exchangers can be high enough to inhibit the practical application of a TEG. Even with an acceptable price of heat exchangers, the cost-performance rather than only the performance of TEGs should be carefully examined for more persuasive comparisons among different TEG modules or between TEGs and other energy sources.

### 3.2. Optimization for the cost performance

With the optimized cross-sectional area ratios $A_n/A_p$, the TEG leg length $l$ can be adjusted to search for the lowest cost-performance ratio. The second type of boundary conditions are implemented with the TEG hot side held at temperature of 1000 K while changing the heat transfer coefficients of the cold side. In addition, the cooling temperature of the heat sink is fixed at 276 K. For a specific assembly and TEG leg length $l$, there exists a heat transfer coefficient $h$ that is sufficient to cool the cold side of the TEG module down to a targeted cold-side temperature, such as 300 K. Such values of the heat transfer coefficients will help maintain the appropriate temperature difference across the TEG, ensuring that the potential of selected TE materials can be fully realized. Fig. 7 displays the evolutions of cold side temperature and output power density with respect to the variation of the heat transfer coefficient. The temperature of cold side decreases rapidly before approaching the temperature of the heat sink. Further increasing the heat transfer coefficient is no longer effective in reducing the temperature. The output power density escalates with the growth of the heat transfer coefficient but enters a saturation region when the descending of the temperature stagnates. From Eq. (3), dwindling the length of TEG legs can stimulate the increment of the output power when $\Delta T$ is unchanged. With TEG leg length as a tunable parameter, the ratio of the heat transfer coefficient to the power generated is appraised for all four assemblies.

As shown in Fig. 8, heat transfer coefficients arise more rapidly than the output power density, revealed by the trend of the $h/P$ curves (green solid pentagons). These results predicate that greater output power is attainable at the expense of more efficient heat exchangers. In other words, the superior output power is correlated with the higher cost. Moreover, TEGs with n-type 2 (Yb-filled SKD + HHs) require considerably larger heat transfer coefficients for generation of the same amount of power as compared with TEG modules involving n-type 1 (Chalcogenides and SiGe). For example, in order to produce 20 W of electricity, assemblies of "p-type 1 + n-type 1" and "p-type 2 + n-type 1" demand heat transfer coefficients of $\sim 1 \times 10^4$ Wm$^{-2}$ K$^{-1}$, while assemblies of "p-type 1 + n-type 2" and "p-type 2 + n-type 2" desire heat transfer coefficients of $\sim 4 \times 10^4$ Wm$^{-2}$ K$^{-1}$. It should be mentioned that the heat transfer coefficient of the forced water convection is in the range of 300–10,000 Wm$^{-2}$ K$^{-1}$. But this doesn't deny the possibility of segmenting the Yb-filled SKD and HHs. In our simulation, the value of fill factor ($F = A_{TE}/A_{HX}$) falls in the range between 0.30 and 0.41. NASA has successfully installed GPHS-RTG with F = 0.034, indicating that ceramic plates in our modelling can be ~10 times larger for alleviating the burden of the heat transfer coefficient by ten-fold.

With obtained optimized dimensions, output power, corresponding heat transfer coefficients, and various prices listed in both the Tables 1 and 2 as well, the cost-performance ratios for the four different assemblies of TEGs can be evaluated as described in Section 2.2. The ideal operating temperature range is from 300 K to 1000 K. Although maintaining 300 K at cold-side is challenging, this temperature configuration is used as benchmark for the selected TE materials. The unit price of heat exchanging system is taken to be 2.05 \$ W$^{-1}$ K for this step. As presented in Fig. 9, the efficiencies almost stay the same with different TEG leg length until the legs are too short when the contact resistances start to become comparable to resistances of the TE materials. On the other hand, the output power density decreases monotonically with the increasing of TEG leg length when temperature difference is kept constant, which is consistent with Eq. (3). The curves of cost-performance ratios show returning points at optimal TEG leg lengths around which wide plateaus exist. For example, TEG with p-type 2 and n-type 1 (Fig. 9c) can achieve the lowest cost-performance ratio of 0.97 \$ W$^{-1}$ at leg length of 0.7 cm while retaining an efficiency of 19.7% and supplying a power density of 3.2 Watt cm$^{-2}$. Assembly of "p-type 1 + n-type 1" (Fig. 9a) comes second with a slightly higher cost-performance ratio of 0.99 \$ W$^{-1}$, possibly attributing to more TE-TE interfaces it have. On the contrary, segmented TEGs with n-type 2 (Yb-filled

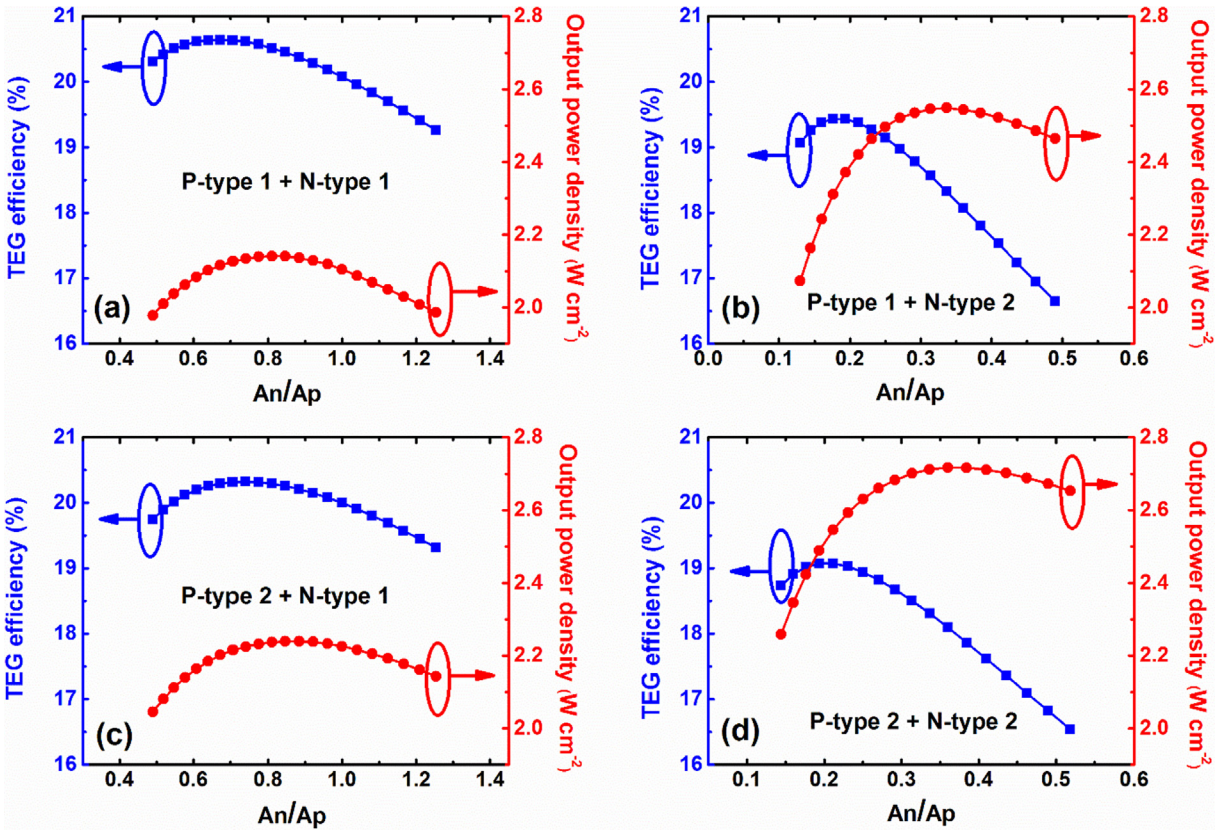


**Fig. 6.** Optimal $A_n/A_p$ ratio for the highest output power densities and corresponding TEG efficiencies for different assemblies of two p-type legs and two n-type legs.

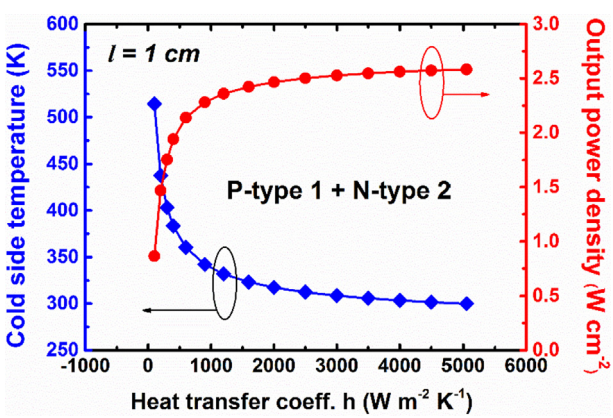


**Fig. 7.** Cold side temperatures and output power densities of a TEG module versus the heat transfer coefficients at the cold side.

SKD + HHs) (Fig. 9b and d) reach cost-performance as low as 1.47 \$ W$^{-1}$ at leg length of 1.3 cm, with efficiency of 18.1% and output power density of 2.2 Watt cm$^{-2}$, despite of their much larger power factors. These results imply that TE materials with higher *ZTs* are more profitable than those with larger power factors.

In reality, it is challenging to maintain a cold-side temperature of 300 K for high temperature applications. The more economical approach is to allow the cold side temperature to increase [46,47]. Fig. 10 shows optimized cost-performance ratios with corresponding TEG efficiencies and output power densities at various cold-side temperatures but fixed hot-side temperature at 1000 K. The unit price of heat exchanging system is chosen to be 10 \$ W$^{-1}$ K, which is closer to the current price compared to 2.05 \$ W$^{-1}$ K. It can be seen that the efficiency drops with the increase of the cold-side temperature, which is easy to understand since the Carnot efficiency decreases with the reduction of the temperature difference across the TEGs. However, the output power densities surprisingly rise with the declined temperature differences. The reason is that for a specific assembly of TE groups, saying "p-type 2 + n-type 1", the optimal geometries at different temperature configurations are not the same, especially the optimized leg length. According to Eq. (3), if the diminution of the leg length outpaced the reduction of the temperature difference, the heat flux density and output power density will escalate. The cost-performance ratios experience a fast descending trend with the ascending temperature of the TEG cold-side, due to the reducing level of heat transfer coefficients. It should be pointed out that both the trends of the output power densities and cost-performance ratios won't last infinitely and will see returning points at some higher temperature of the TEG cold side, when the decline of the cost will be overtaken by the reduction of the power generation. After all, the cost-performance ratios of segmented TEGs in this study can reach the benchmark of 1 \$ W$^{-1}$ at $T_C$ = 373 K. The assemblies of "p-type 1 + n-type 1" and "p-type 2 + n-type 1" can achieve 0.88 \$ W$^{-1}$ and 0.86 \$ W$^{-1}$, respectively. In contrast, assemblies of "p-type 1 + n-type 2" and "p-type 2 + n-type 2" can attain 1.13 \$ W$^{-1}$ and 1.11 \$ W$^{-1}$, respectively. Corresponding to the lowest cost-performance ratio of 0.86 \$ W$^{-1}$ with the unit price of heat exchangers at 10 \$ W$^{-1}$ K, assemblies of "p-type 2 + n-type 1" could provide power densities of 3.0 Watt cm$^{-2}$ with efficiency of 17.8%. These results indicate that the segmented TEGs have the potential to compete with other types of power generation methods, such as photovoltaic cells. The ~1 \$ W$^{-1}$ capability of the high-performance segmented TEGs announces the financial feasibility and competitiveness of the thermoelectric technology.

## 4. Conclusion

Segmented TEG modules are constructed by currently high-performance TE materials, including various Chalcogenides, SiGe alloy,

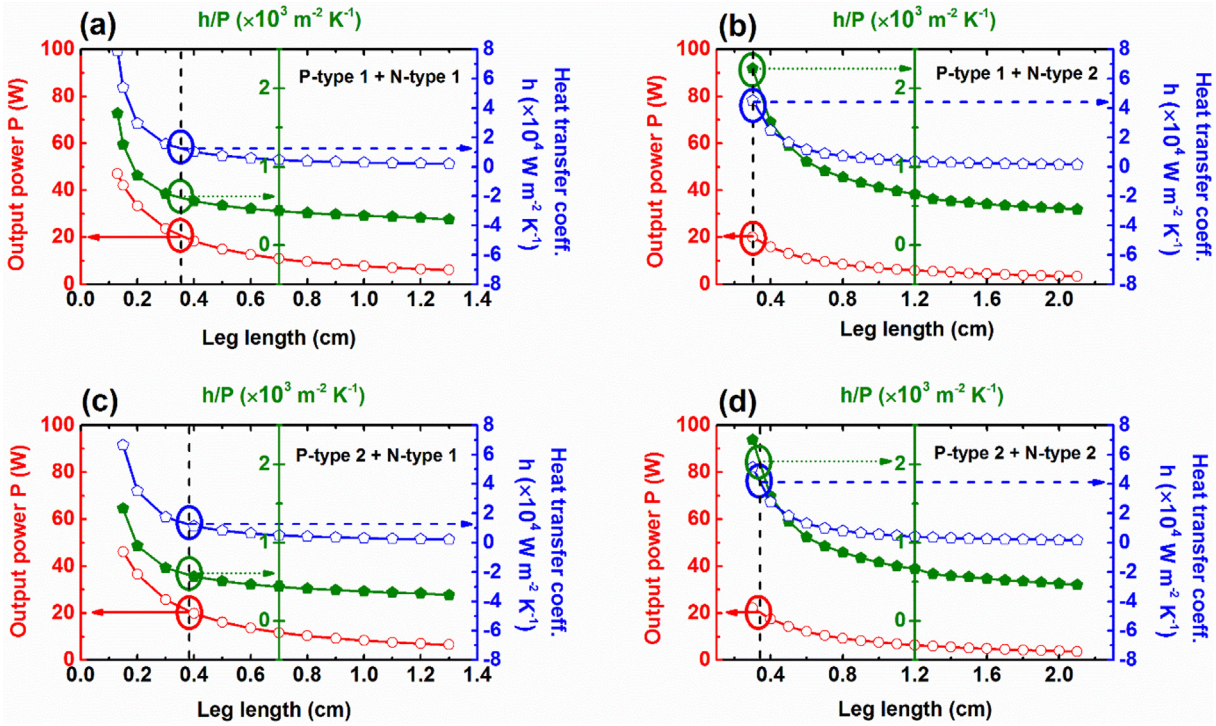


**Fig. 8.** Output power and corresponding heat transfer coefficients versus leg lengths of TEGs.

Skutterudites and Half-Heuslers. These TE materials are prudently chosen based on an overall consideration of the TE figure of merit (*ZT*), compatibility factors and power factors. Four different segmented TEG modules are built up by assembling two groups of p-type TE materials and two groups of n-type TE materials. 3D finite-element analysis with ANSYS was conducted for systematical modelling of these segmented TEG modules. All the temperature-dependent TE properties were extracted directly from the published experimental data, covering a temperature range from 300 K to 1000 K. Contact effects including the electrical and thermal contact resistances are also considered, at both

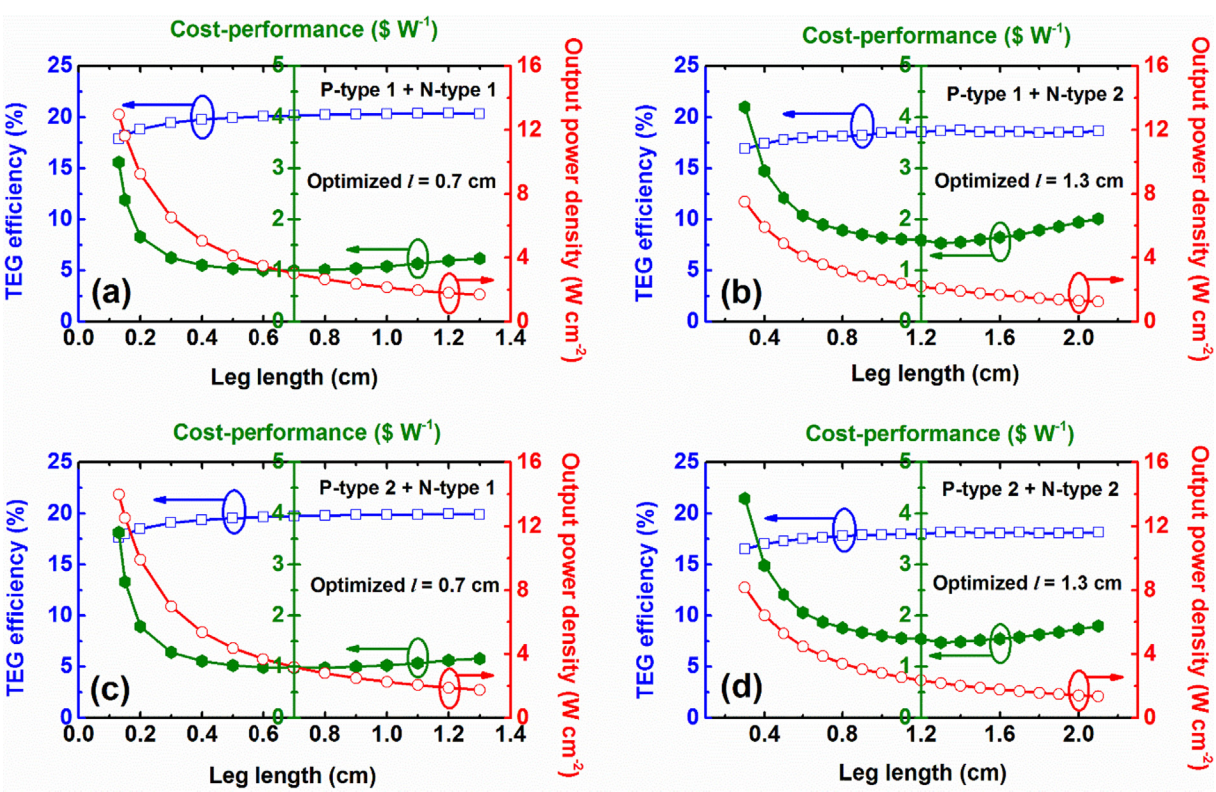


**Fig. 9.** Cost-performance ratios, TEG efficiencies and output power densities versus leg lengths of different TEG modules. The temperatures of cold side and hot-side are fixed at 300 K and 1000 K, respectively. The unit price of 2.05 $ $W^{-1}$ K for heat exchangers is used here.

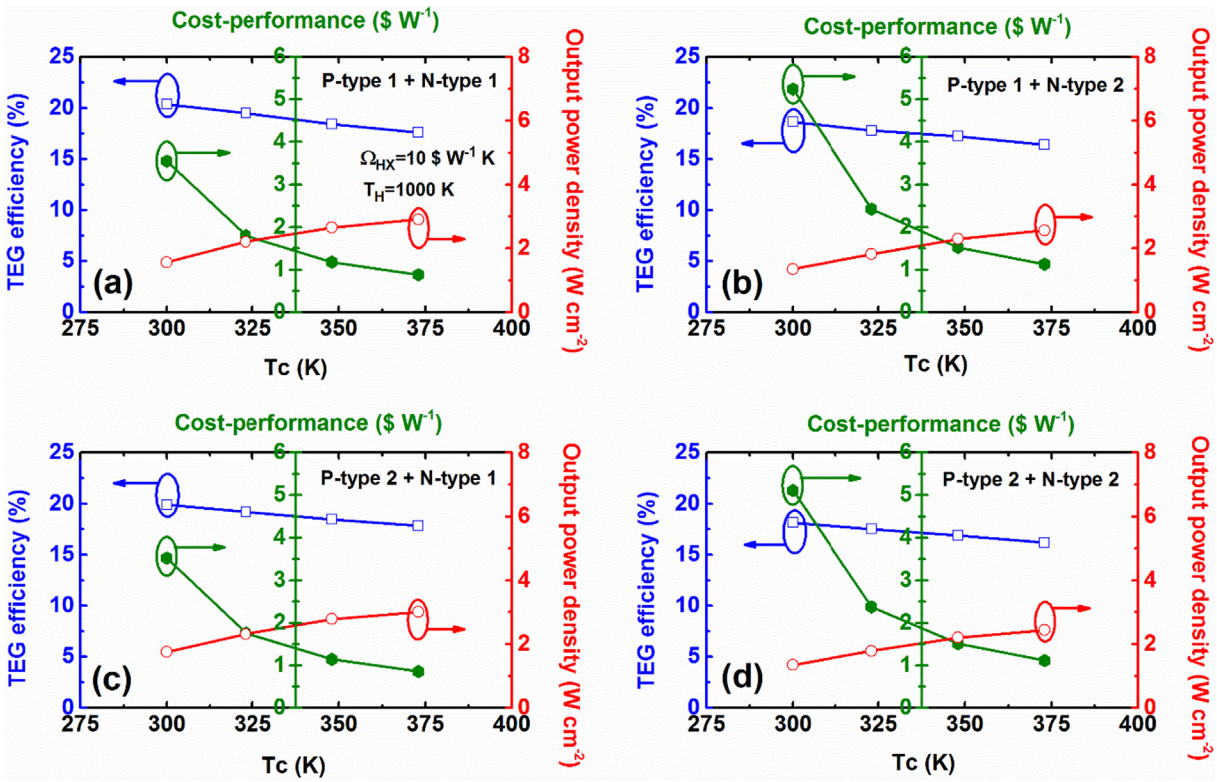


**Fig. 10.** Cost-performance ratios, TEG efficiencies and output power densities versus different cold-side temperature and fixed hot-side temperature at 1000 K. The unit price of 10 $ $W^{-1}$ K for heat exchangers is used here.

the TE-TE and TE-electrode interfaces. Two kinds of boundary conditions (BCs) are imposed, with type I representing the temperature of 1000 K at hot side versus 300 K (323 K, 348 K, 373 K) at cold end of TEG modules and type II having 1000 K held at hot sides while varying the heat transfer coefficients of cold sides. These two classes of BCs are adopted to discover the optimal TEG leg cross-sectional area ratios ($A_n/A_p$) and optimum leg lengths of TEG modules, respectively. The results show that the TE materials with high power factors, such as Yb-filled SKD and HHs, are preferred only for the applications in which cost is not a major concern. When expenses are taken into account, successful segmentation of high-*ZT* TE materials exhibit remarkable advantages: a cost-performance ratio of ~0.86 $ $W^{-1}$ with an efficiency of 17.8% and a power density of 3.0 Watt $cm^{-2}$ have been demonstrated. On the other hand, their rivals with larger power factors can only make segmented TEG modules capable of offering a cost-performance ratio of ~1.11 $ $W^{-1}$, efficiency of 16.2% and output power density of 2.4 Watt $cm^{-2}$. The demonstrated low cost-effectiveness, high efficiency and large output power density are a perfect match for high temperature applications such as automobiles, aircrafts and industrial furnaces. The design method and procedure shown in this study can serve as a guidance to the planning and implementation of cost-effective TEG systems. More importantly, these results not only confirm *ZT* as the number one criterion for selecting TE materials, but also forecast the commercial viability and competitiveness of segmented TEGs in the same metrics as other renewable energy sources.

## Author contributions

D.L. guided and supervised the project. Z.O. conducted the numerical simulation. All authors analysed the results and reviewed the manuscript.

## Additional information

Competing financial interests: the authors declare no competing financial interests.

## Acknowledgments

This work was partially supported by National Science Foundation ECCS-1151140.

## References

[1] Rowe DM. Thermoelectrics handbook: macro to nano. CRC Press; 2005.
[2] Snyder GJ. Small thermoelectric generators. Electrochem Soc Interface 2008;17:54.
[3] Fisk LA. Journey into the unknown beyond. Science 2005;309:2016–7.
[4] Smith CJW, Cahill JS, Nuhoglu A. Macro to nano: scaling effects of Bi2Te3 thermoelectric generators for applications in space. PAM Rev: Energy Sci Technol 2016;3:86–99.
[5] Gayner C, Kar KK. Recent advances in thermoelectric materials. Prog Mater Sci 2016;83:330–82.
[6] Twaha S, Zhu J, Yan Y, Li B. A comprehensive review of thermoelectric technology: materials, applications, modelling and performance improvement. Renew Sustain Energy Rev 2016;65:698–726.
[7] Tritt TM, Subramanian M. Thermoelectric materials, phenomena, and applications: a bird's eye view. MRS Bull 2006;31:188–98.
[8] Bell LE. Cooling, heating, generating power, and recovering waste heat with thermoelectric systems. Science 2008;321:1457–61.
[9] Zhao L-D, et al. Ultralow thermal conductivity and high thermoelectric figure of merit in SnSe crystals. Nature 2014;508:373–7.
[10] Xie W, et al. Identifying the specific nanostructures responsible for the high thermoelectric performance of (Bi, Sb)$_2$Te$_3$ nanocomposites. Nano Lett 2010;10:3283–9.
[11] Zhao H, et al. High thermoelectric performance of MgAgSb-based materials. Nano Energy 2014;7:97–103.
[12] Wu H, et al. Broad temperature plateau for thermoelectric figure of merit ZT > 2 in phase-separated PbTe0.7S0.3. Nat Commun 2014;5:4515.
[13] Zhao L-D, et al. Ultrahigh power factor and thermoelectric performance in hole-doped single-crystal SnSe. Science 2016;351:141–4.
[14] Liu WS, et al. Thermoelectric property studies on Cu-doped n-type CuxBi2Te2.7Se0.3 nanocomposites. Adv Energy Mater 2011;1:577–87.
[15] Hsu KF, et al. Cubic AgPbmSbTe$_{2+m}$: bulk thermoelectric materials with high figure

of merit. Science 2004;303:818–21.
[16] Basu R, et al. Improved thermoelectric performance of hot pressed nanostructured n-type SiGe bulk alloys. J Mater Chem A 2014;2:6922–30.
[17] Meng X, et al. Grain boundary engineering for achieving high thermoelectric performance in n-type Skutterudites. Adv Energy Mater 2017;7:1602582.
[18] Kim KS, et al. Direct observation of inherent atomic-scale defect disorders responsible for high-performance $Ti_{1-x}Hf_xNiSn_{1-y}Sb_y$ Half-Heusler thermoelectric alloys. Adv Mater 2017;29:1702091.
[19] Goldsmid HJ. Introduction to thermoelectricity, vol. 121. Springer Science & Business Media; 2009.
[20] Xiao J, Yang T, Li P, Zhai P, Zhang Q. Thermal design and management for performance optimization of solar thermoelectric generator. Appl Energy 2012;93:33–8.
[21] Liang X, et al. Comparison and parameter optimization of a two-stage thermoelectric generator using high temperature exhaust of internal combustion engine. Appl Energy 2014;130:190–9.
[22] Liu Z, et al. Geometry optimization of two-stage thermoelectric generators using simplified conjugate-gradient method. Appl Energy 2017;190:540–52.
[23] Snyder GJ. Application of the compatibility factor to the design of segmented and cascaded thermoelectric generators. Appl Phys Lett 2004;84:2436–8.
[24] Ali H, Yilbas BS, Al-Sharafi A. Innovative design of a thermoelectric generator with extended and segmented pin configurations. Appl Energy 2017;187:367–79.
[25] Snyder GJ, Ursell TS. Thermoelectric efficiency and compatibility. Phys Rev Lett 2003;91:148301.
[26] Ouyang Z, Li D. Modelling of segmented high-performance thermoelectric generators with effects of thermal radiation, electrical and thermal contact resistances. Sci Rep 2016;6:24123.
[27] Liu W, Yan X, Chen G, Ren Z. Recent advances in thermoelectric nanocomposites. Nano Energy 2012;1:42–56.
[28] Alam H, Ramakrishna S. A review on the enhancement of figure of merit from bulk to nano-thermoelectric materials. Nano Energy 2013;2:190–212.
[29] Rogl G, Rogl P. Skutterudites, a most promising group of thermoelectric materials. Curr Opin Green Sustain Chem 2017;4:50–7.
[30] Huang L, et al. Recent progress in half-Heusler thermoelectric materials. Mater Res Bull 2016;76:107–12.
[31] Ngan PH, et al. Towards high efficiency segmented thermoelectric unicouples. Phys Status Solidi A 2014;211:9–17.
[32] McEnaney K, Kraemer D, Ren Z, Chen G. Modeling of concentrating solar thermoelectric generators. J Appl Phys 2011;110:074502.
[33] Zhang Q, et al. Realizing a thermoelectric conversion efficiency of 12% in bismuth telluride/skutterudite segmented modules through full-parameter optimization and energy-loss minimized integration. Energy Environ Sci 2017;10:956–63.
[34] Yee SK, LeBlanc S, Goodson KE, Dames C. $ per W metrics for thermoelectric power generation: beyond ZT. Energy Environ Sci 2013;6:2561–71.
[35] LeBlanc S, Yee SK, Scullin ML, Dames C, Goodson KE. Material and manufacturing cost considerations for thermoelectrics. Renew Sustain Energy Rev 2014;32:313–27.
[36] Rezania A, Rosendahl L, Yin H. Parametric optimization of thermoelectric elements footprint for maximum power generation. J Power Sources 2014;255:151–6.
[37] Kim H, Kim W. A way of achieving a low $/W and a decent power output from a thermoelectric device. Appl Energy 2015;139:205–11.
[38] Benday NS, Dryden DM, Kornbluth K, Stroeve P. A temperature-variant method for performance modeling and economic analysis of thermoelectric generators: Linking material properties to real-world conditions. Appl Energy 2017;190:764–71.
[39] Chen S, Ren Z. Recent progress of half-Heusler for moderate temperature thermoelectric applications. Mater Today 2013;16:387–95.
[40] Hendricks TJ, Yee S, LeBlanc S. Cost scaling of a real-world exhaust waste heat recovery thermoelectric generator: a deeper dive. J Electron Mater 2016;45:1751–61.
[41] Hazan E, Ben-Yehuda O, Madar N, Gelbstein Y. Functional graded germanium-lead chalcogenide-based thermoelectric module for renewable energy applications. Adv Energy Mater 2015;5:1500272.
[42] Hu X, et al. Power generation from nanostructured PbTe-based thermoelectrics: comprehensive development from materials to modules. Energy Environ Sci 2016;9:517–29.
[43] Joshi G, Poudel B. Efficient and robust thermoelectric power generation device using hot-pressed metal contacts on nanostructured half-Heusler alloys. J Electron Mater 2016;45:6047–51.
[44] Fu C, et al. Realizing high figure of merit in heavy-band p-type half-Heusler thermoelectric materials. Nat Commun 2015;6:8144.
[45] Zhou H, et al. Low interface resistance and excellent anti-oxidation of Al/Cu/Ni multilayer thin-film electrodes for Bi2Te3-based modules. Nano Energy 2017;40:274–81.
[46] He R, et al. Achieving high power factor and output power density in p-type half-Heuslers Nb1-xTixFeSb. Proc Natl Acad Sci 2016;113:13576–81.
[47] Kim HS, Liu W, Chen G, Chu C-W, Ren Z. Relationship between thermoelectric figure of merit and energy conversion efficiency. Proc Natl Acad Sci 2015;112:8205–10.